



# Hydrogen trapping and hydrogen embrittlement of Mg alloys

M. Kamilyan<sup>1</sup>, R. Silverstein<sup>1,\*</sup>, and D. Eliezer<sup>1</sup>

<sup>1</sup>Department of Materials Engineering, Ben-Gurion University of the Negev, Beer-Sheva, Israel

Received: 13 March 2017

Accepted: 3 June 2017

Published online:  
12 June 2017

© Springer Science+Business  
Media, LLC 2017

## ABSTRACT

In this paper, the effect of local hydrogen concentration and distribution in magnesium (Mg) alloys is studied in regard to hydrogen embrittlement. Quantitative studies of hydrogen trapping sites and release behavior in AZ91 and AZ31 magnesium alloys are being studied by thermal desorption analysis (TDS). The trapping energy levels are used to discuss the embrittlement mechanisms due to their control on hydrogen availability. The embrittlement process is caused by hydrogen in combination with residual or applied stress and can lead to the mechanical degradation of a material. The susceptibility of Mg alloys is directly related to the role of the second phases controlling the hydrogen trapping mechanisms. In this work, we examine the effect of Mg's microstructure on the magnesium hydride (MgH<sub>2</sub>) reaction, referred to as hydriding, and its decomposition, referred to as dehydriding. The MgH<sub>2</sub> compound was investigated in regard to two aspects: first, as the main source for controlling the hydrogen dehydriding process; second, as a hydrogen trapping site for preventing hydrogen embrittlement process. The TDS analysis was used to study the hydrogen trapping mechanisms by studying the traps' density and distribution and relating them to potential lattice defects. The TDS analysis revealed a certain hydrogen concentration evolving near  $\beta$ -Mg<sub>17</sub>Al<sub>12</sub> phase, accompanied by H<sub>2</sub> desorption at a temperature range between ~200 and 300 °C. It is proposed that  $\beta$ -phase plays a fundamental role in the dehydriding process, and this response is a crucial step in effecting the embrittlement behavior.

## Introduction

Structural magnesium (Mg) alloys offer desirable properties such as low density, dimensional stability, machinability, and high specific strength. These properties make Mg alloys advantageous for use in

many structural applications, such as in the automotive, aerospace, and electronic industries [1–3].

However, the susceptibility of Mg alloys to premature intergranular cracking can lead to low ductility and low fracture toughness at room temperature, thus limiting their widespread

Address correspondence to E-mail: barrav@post.bgu.ac.il

applications [4, 5]. The reduction of these properties can be due to hydrogen, often in combination with residual or applied stress known as hydrogen fracture mechanism or hydrogen embrittlement [6–8].

The susceptibility of Mg alloys to the hydrogen embrittlement phenomenon is mostly affected by second phases, Mg hydrides ( $\text{MgH}_2$ ), and their binding energy with hydrogen [4, 6, 9]. In some of our different publications, we have already proved that one of the main factors controlling the embrittlement process in metals is second phases, due to their strong binding energy with hydrogen [10–15].

In this paper, we refer to the role of Mg's microstructure and, specifically, to  $\beta\text{-Mg}_{17}\text{Al}_{12}$  phase, in  $\text{MgH}_2$  reaction (hydriding) and its decomposition (dehydriding). In particular, we studied the microstructure's effect on the formation, stability, content, and binding energy of  $\text{MgH}_2$  with Mg second phases (trapping sites for hydrogen). This paper presents the effect of  $\beta\text{-Mg}_{17}\text{Al}_{12}$  phase as a hydrogen embrittlement controller and as a potential hydrogen second-phase trapping site.

According to previously published works, modification of the Mg crystal structure and microstructure has become the main purpose for greatly improving the kinetics of  $\text{MgH}_2$  [16–18] and the corrosion resistance [1, 19, 20], and this trend seems to be very prospective. In this research, we study the possible hydrogen trapping states in occupation sites (lattice's defects), especially in second phases on dehydriding reaction and on hydrogen embrittlement. This study was possible using thermal desorption spectrometry (TDS) analysis, in which desorbed hydrogen is measured during a non-isothermal heating. The significance of using TDS is the possibility of identifying different types of trapping sites and for the measurement of their binding energy and density.

In this work, we compare between die-cast magnesium–aluminum–zinc (AZ) alloy (AZ91) and rolled plate AZ31, which has a different additive of Al and a different microstructure. The main difference in these two fabrication techniques is the obtained ductility. Die-cast alloys can reach up to  $\sim 3\%$  ductility compared with rolled alloys, which achieve five times higher ductility ( $\sim 15\%$  higher ductility) [21]. This fact, along with their absence of casting defects and better mechanical properties, makes wrought Mg alloys preferable for the enhancement of the dehydriding process.

## Experimental procedure

### Materials

The chemical compositions of magnesium–aluminum–zinc (AZ)—AZ91 and AZ31—are listed in Table 1, as reported by the manufacturer.

In this study, die-cast rods AZ91 and rolled sheet AZ31 were cut to plates with the following sizes: 10 mm diameter for AZ91 and  $10 \times 5$  mm for AZ31, with a thickness of 1 mm for both. The samples were pre-charged with hydrogen at high pressure and high temperature (gas-phase charging) in a hydrogen gas tank. Gas-phase charging was conducted at 30 MPa and  $300^\circ\text{C}$  for 14 h (h). These charging conditions were chosen in order to create a homogeneous hydrogen content along the metal's bulk and was inspired by our previous work [11, 22]. Charging conditions were estimated according to the thin plate solution of Fick's second law [23], where the effective diffusion at room temperature,  $D_{\text{H\_in\_Mg}} \approx 4.061 \times 10^{-10} \text{ m}^2/\text{s}$ , was taken according to Atrens et al. [24]. These charging conditions allowed for a homogeneous hydrogen content of  $\sim 100\%$ wt ppm.

### Microstructure analysis

The Mg microstructures, before and after the gas-phase charging, were examined using the following microstructural observations: scanning electron microscopy (SEM), energy-dispersive spectrometry (EDS), optical microscopy (OM), and X-ray diffraction (XRD) with  $\text{Cu-K}_\alpha$  radiation ( $\lambda = 1.54 \text{ \AA}$ ). Samples were etched in a solution of acetic acid/water/ethanol to 1:1:7 parts with 4.2 gr picric acid. The final stage included ultrasonic cleaning in acetone and ethanol.

### Thermal desorption spectrometry (TDS)

For the investigation of hydrogen interaction with metal defects and second phases, a thermal

**Table 1** Chemical composition of the investigated die-cast AZ91 and rolled AZ31 Mg alloys (%wt)

Sample	Al	Zn	Mn	Cu	Ni	Fe	Mg
AZ91	9.0	0.7	0.13	0.30	0.002	0.005	Bal
AZ31	3.0	1.0	0.40	0.04	0.005	0.005	Bal

desorption process was conducted. This procedure includes a non-isothermal heating under ultra-high vacuum (UHV)  $\sim 10$   $\mu\text{Pa}$  of gas-phase charged samples. A plot of hydrogen desorption rate versus temperature is achieved for three constant heating rates: 2, 4, and 6  $^{\circ}\text{C}/\text{min}$ . The working procedure, as described elsewhere [10, 11, 25, 26], allows for the identification of different types of traps which coexist in the specimen.

Activation energies of hydrogen interactions with trapping sites were determined according to Lee and Lee's model [27, 28], where hydrogen desorption rate is described by:

$$dx/dt = A(1 - X)\exp(-E_a/RT_c), \quad (1.1)$$

where  $X$  is the hydrogen content that escapes from a trap,  $A$  is the reaction rate constant,  $E_a = E_b + E_Q$  is the activation energy for releasing hydrogen from its trapping site and it is the sum of binding energy ( $E_b$ ) and the activation energy needed for diffusion ( $E_Q$ ) through the lattice interstitial sites,  $R$  is the gas constant, and  $T_c$  is the desorption temperature.

$E_a$  is extracted for each peak in the TDS spectrum by referring to the temperature's shift in a TDS peak when increasing the heating rate. The dependence of a certain peak on the heating rate is described by:

$$d\ln(\varphi/T_c^2)/d(1/T_c) = -E_a/R, \quad (1.2)$$

where  $\varphi$  is the heating rate.

$E_a$  is extracted for a certain peak by the linear slope of  $\ln(\varphi/T_c^2)$  versus  $1/T_c$ .

## Results and discussion

### XRD and microstructure analysis

#### Hydrogen interaction with die-cast AZ91

Microstructural changes of hydrogen in AZ91 were examined by XRD and microstructural observations. The XRD diffraction patterns in Fig. 1 show a comparison between non-charged AZ91, gas-phase charged AZ91, and gas-phase charged AZ91 after non-isothermal heating (at 2  $^{\circ}\text{C}/\text{min}$ ) to 300  $^{\circ}\text{C}$ . As expected, the non-charged AZ91 sample showed a combined crystal structure of primary  $\alpha$ -Mg phase, with hexagonal crystal structure, along with aluminum magnesium phase ( $\beta$ - $\text{Mg}_{17}\text{Al}_{12}$  phase), with an A12-type structure. Gas-phase hydrogen charging

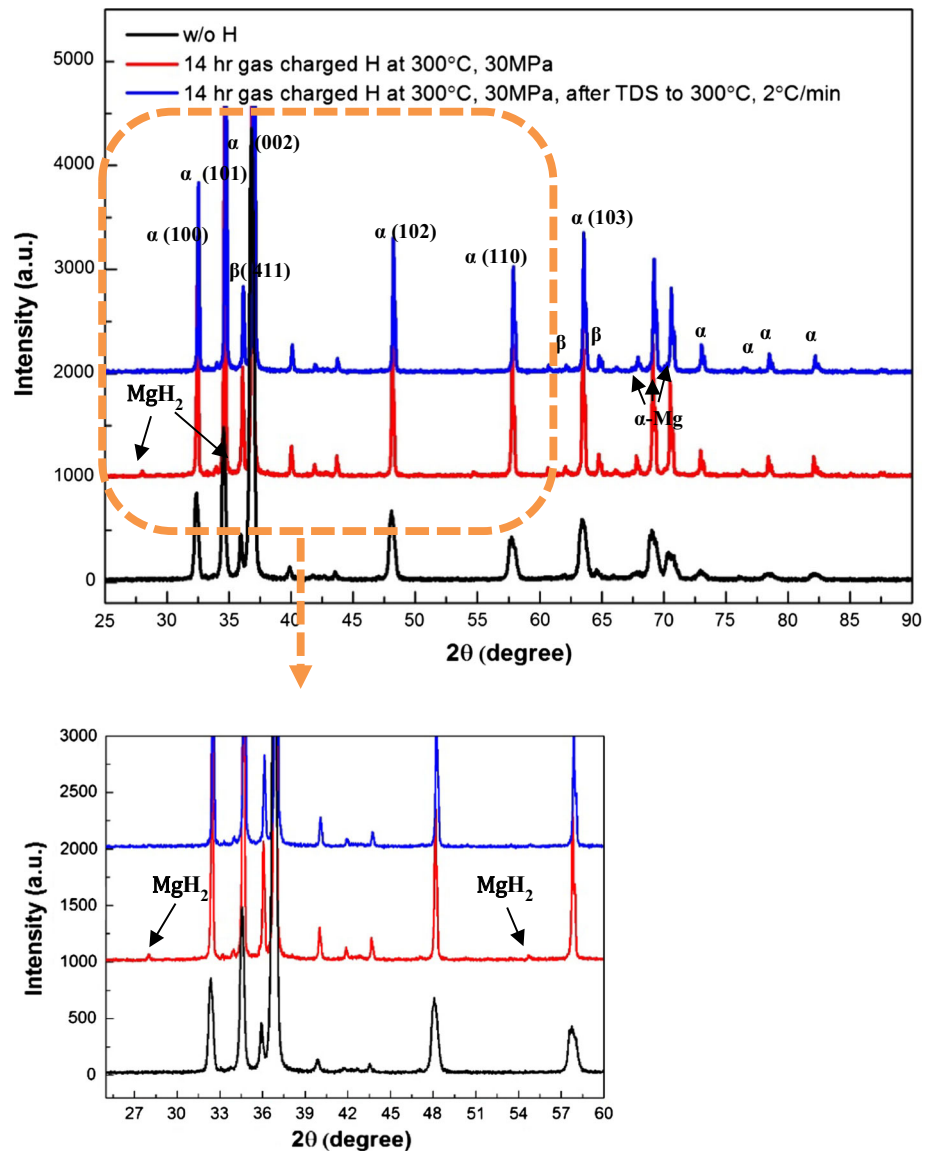
resulted in the formation of  $\text{MgH}_2$  with a tetragonal crystal structure. The thermal desorbed gas-phase spectrum indicates a partial decomposition of  $\text{MgH}_2$  at 300  $^{\circ}\text{C}$ , though it is literarily known [1, 29] that decomposition temperature is usually 300  $^{\circ}\text{C}$  at 101.3 kPa  $\text{H}_2$  pressure. These results are supported by the SEM micrographs, Fig. 2, showing the starting microstructure of non-charged AZ91, Fig. 2a, compared with gas-phase charged AZ91, Fig. 2b. The formation of micro-cracking along  $\beta$ -phase is clearly seen from Fig. 2b and seems to be intergranular. From the backscattered SEM micrograph, Fig. 2c, it can be seen that  $\text{MgH}_2$  is formed adjacent to  $\beta$ -phase. Supported by the work of Chen et al. [30], it can be said that these darkest areas can also refer to the formation of a hydrogen gas molecule ( $\text{H}_2$ ) inside a blister. A comparison between the secondary SEM micrograph, Fig. 2d, and the backscattered SEM micrograph, Fig. 2c, supports this indication. From EDS, we have found that Point 1 consists of 93 wt% Mg, 3 wt% Al, and 4%wt O. Furthermore, Point 2 consists of 92.5 wt% Mg, 4.5 wt% Al and 3%wt O, and Point 3 consists of 99 wt% Mg and 1 wt% O. This means that Point 3 presents the  $\text{MgH}_2$  phase.

According to the work of Chen et al. [31], the reason for cracking could be related to the formation of a hydrogen gas ( $\text{H}_2$ ) molecule inside a blister in  $\beta$ -phase, leading to high pressure and, thus, cracking. An additional explanation is related to the lattice expansion of Mg by  $\text{MgH}_2$ , leading to higher internal stress which then cracks  $\beta$ -phase [32]. In this Mg alloy, the embrittlement process was ascribed to lattice expansion by  $\text{MgH}_2$ . Using WinPLOT-RXD analysis, we compared the lattice parameters of Mg with those of  $\text{MgH}_2$  and calculated an increment of  $\sim 30\%$  in the Mg lattice volume. Therefore, it can be said that  $\text{H}_2$  was able to promote cracking.

#### Hydrogen interaction with rolled AZ31

In order to examine the effect of Al's addition and fabrication method on  $\text{MgH}_2$ 's formation and stability, AZ31 was chosen. This Mg alloy shows a combined crystal structure of  $\alpha$ -Mg, along with eutectic Mg phase ( $\alpha$ -Mg +  $\beta$ - $\text{Mg}_{17}\text{Al}_{12}$ ) and aluminum manganese (AlMn) phase with a tetragonal crystal structure; crystal structure was confirmed by EDS measurements. The XRD spectrum of the non-charged sample, Fig. 3, did not show any traces for  $\beta$ -phase, as opposed to the AZ91D results. The reason is

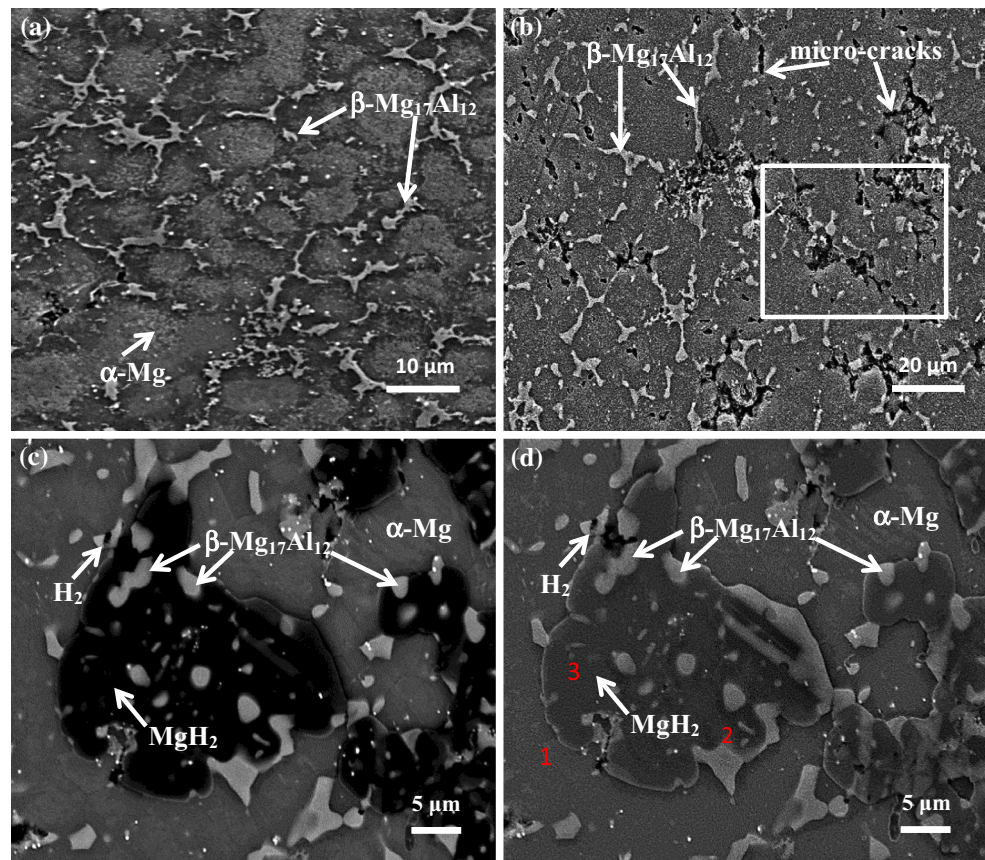
**Figure 1** XRD pattern of AZ91 samples: non-charged, gas-phase charged for 14 h at 30 MPa and 300 °C, and non-isothermal (2 °C/min) desorbed gas-phase charged heated for 300 °C.



probably due to the lower amount of Al additive (3 wt% Al). At low Al addition of  $\sim 2$  wt%, the two eutectic phases participate at  $\alpha$ -Mg grain boundaries; only at higher Al additives ( $\geq 6$  wt%) does  $\beta$ -phase tend to participate distinctly [33]. This fact explains the difficulty of detecting  $\beta$ -phase at lower Al addition. Moreover, according to the Lever rule [34], it is clearly understood that a higher amount of Al in the eutectic phase range will lead to a higher  $\beta$ -phase content. This indication can be clearly seen from the OM micrographs in Figs. 4a and b, which show the appearance of eutectic Mg phase. An additional interesting observation is the complete decomposition of  $\text{MgH}_2$ , which was seen in the non-isothermal

heating (2 °C/min) to 300 °C, Fig. 3, compared with partial decomposition at AZ91, Fig. 1. The intensity of the primary  $\text{MgH}_2$  peaks in the XRD spectra of gas-phase charged AZ31, Fig. 3, is  $\sim 20\%$  lower than those of gas-phase charged AZ91, Fig. 1. The reason could be related to the lower amount or lack of appearance of  $\beta$ -phase in this alloy. As previously stated, there might be a strong relation between  $\beta$ -phase and  $\text{MgH}_2$  hydriding and dehydriding which is probably related to the hydrogen state and binding energy with  $\beta$ -phase. This statement is in agreement with the minor lattice expansion calculated from the AZ31 XRD spectra, which was less than  $\sim 1\%$  in the  $\alpha$ -Mg lattice. These results are supported by the OM

**Figure 2** Micrographs of AZ91: **a** non-charged and **b, c, d** gas-phase charged for 14 h at 30 MPa and 300 °C showing surface cracking as a result of hydrogen and  $\beta$ -Mg<sub>17</sub>Al<sub>12</sub> phase. The enlargement of the marked square in **(b)** is shown in backscattered SEM **(c)** and secondary SEM **(d)**.



micrograph of gas-phase sample, Fig. 4b, showing the lack of cracking when  $\beta$ -phase content is significantly lower.

### Hydrogen trapping states and activation energy in AZ91 and AZ31

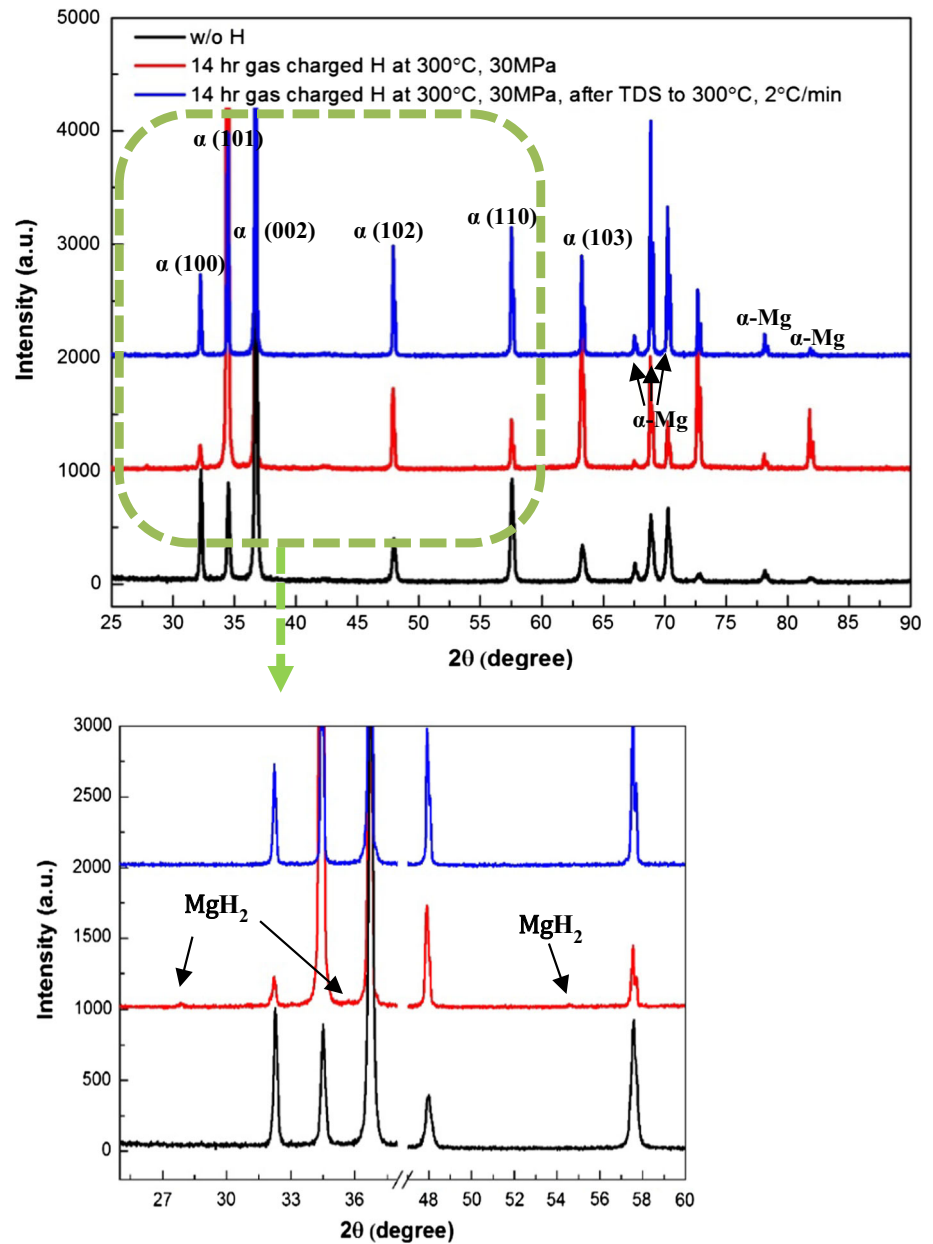
The thermal desorption spectrometry (TDS) spectra of gas-phase charged AZ91 and AZ31, for 14 h at 30 MPa and 300 °C, are presented in Figs. 5a and b, respectively. Each spectrum, which is on the same coordinate system, refers to a different heating rate (2, 4, and 6 °C/min) and is characterized between 4 and 5 peaks. Each peak refers to a certain activation energy (the summation of binding energy + activation energy for hydrogen diffusion was taken as  $E_Q \approx 17$  kJ/mole [24]) of different metal's defects (trapping sites, such as second phases, grain boundary, dislocations) with hydrogen.

Due to diffusion consideration and data process recording of TDS, a higher heating rate shows greater intensity and a higher temperature level for each peak [10, 11, 25].

The main difference between the two spectra of AZ91 and AZ31, Figs. 5a and b, is the straight, narrow peaks, which look like rising noise at the end of each AZ91D spectrum. The range of these narrow peaks is between 145 and 300 °C and is probably related to MgH<sub>2</sub> dehydrating and hydrogen gas molecule (H<sub>2</sub>) desorption. This phenomenon is related to the incoherency between MgH<sub>2</sub> and  $\beta$ -phase [31], leading to the repartition of hydrogen to form H<sub>2</sub>.

Activation energies were calculated by applying Lee and Lee's model [27, 28], Eq. 1.1, which describes hydrogen desorption from the metal's defects (trapping sites for hydrogen). Since, hydrogen is "trapped" in a lattice defect, heating should be involved in order to release it. In this study, we conducted hydrogen desorption measurements by heating the samples up to 300 °C. According to Lee and Lee's model in order to extract the activation energy from Eq. 1.1, the experiment should be repeated at three different heating rates. When heating rate is increased, it can be seen from Fig. 5 in the paper that the peaks are shifting to a higher temperature peak

**Figure 3** XRD pattern of AZ31: non-charged, gas-phase charged for 14 h at 30 MPa and 300 °C, and non-isothermal (2 °C/min) desorbed gas-phase charged heated for 300 °C.



level. The reason is due to the faster kinetics that is needed for hydrogen evaluation. From the shift of each peak, Eq. 1.2 can be built, and by conducting a curve fitting, the slope of Eq. 1.2, which is  $E_a$ , can be extracted.

Curve fittings were built for each individual peak in order to extract its trapping activation energy with hydrogen. The results are listed in Table 2, and accuracy measurements were estimated with a 95% confident interval. The first peak in each spectra, Fig. 5, is neglected due to the invalidity of the Lee and Lee's model at low temperatures [35]. This peak refers to the desorption of dissolved interstitial

hydrogen, a process which is controlled under diffusion only without trapping.

It can be seen from Table 2 that all calculated activation energy values, for both AZ91 and AZ31, are between 28 and 40 kJ/mol. The calculated activation energies can be ascribed to different trapping sites, such as elastic stress field of dislocation, and, at high activation energies, screw's dislocation core or grain boundaries. According to our previously published work on steels [11, 15, 25, 26] and titanium [36, 37], the range of activation energies ascribed to each trapping site is as follows: elastic stress field of dislocation [calculated values range 0–20 kJ/mol],

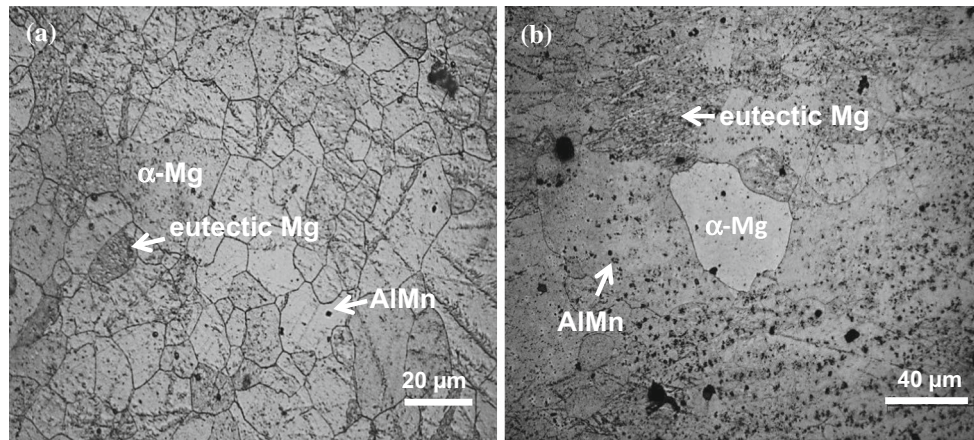


**Figure 4** Micrographs of AZ31: **a** non-charged and **b** gas-phase charged for 14 h at 30 MPa and 300 °C, showing no surface cracking, which results from the significantly lower  $\beta$ -phase content.

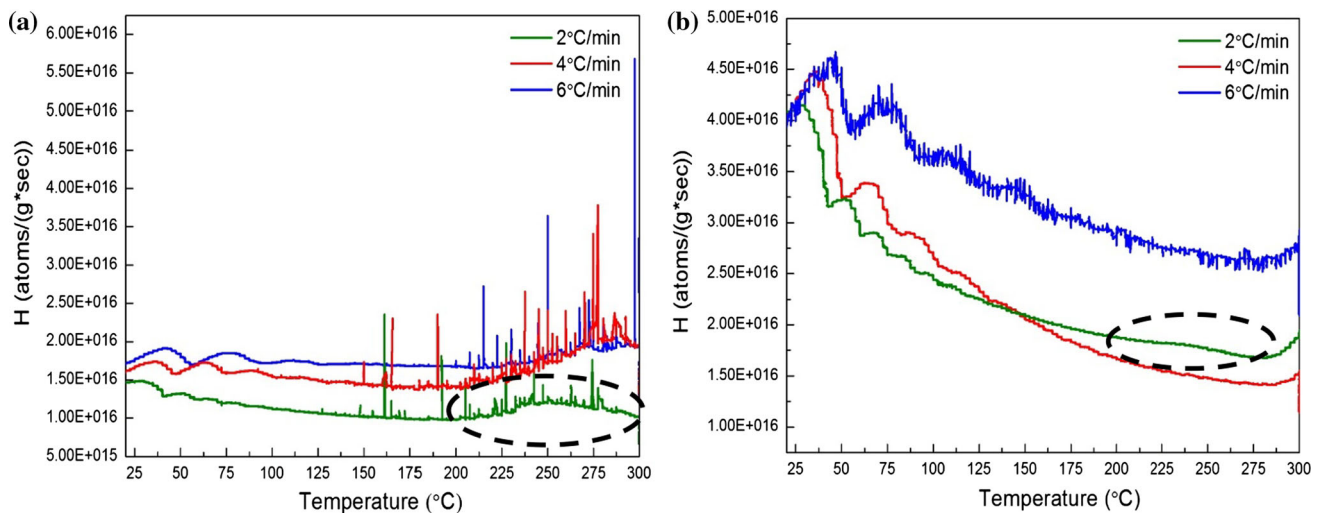


**Figure 5** TDS spectra of gas-phase charged for 14 h at 30 MPa and 300 °C AZ91 (**a**) and AZ31 (**b**).

screw's dislocation core or grain boundaries [calculated values range 20–40 kJ/mol], and high angle boundaries [calculated values range 49–55 kJ/mol]. The last peak in each spectra (peak numbers 4 and 5 for AZ91 and AZ31, respectively) appears only at the lower heating rate (2 °C/min) spectrum and was assumed to relate to the  $\text{MgH}_2$  release and decomposition from  $\beta$ -second phase. According to some of our other work [11, 37], it was already concluded that a high-temperature peak above—200 °C—is usually associated with second phases accompanied by higher activation energies ( $\sim 60$  kJ/mol). An additional interesting observation is the difference in the peaks' shapes and widths. The AZ91 peaks are less broad and have one higher order of magnitude of

intensity. Moreover, the last peaks (marked in black) in the TDS spectra are characterized by additional straight narrow peaks, which are related to  $\text{H}_2$  molecules being trapped between  $\beta$ -phase and the  $\text{MgH}_2$ . When the dehydrating temperature is reached ( $\sim 300$  °C), the  $\text{H}_2$  gas molecules attached to  $\beta$ -phase also desorb out, which explains many jumps when approaching the dehydrating temperature. At AZ31, Fig. 5b, peak number 4 is much smaller in intensity and does not show any additional jumps, probably due to the absence of  $\beta$ -phase. In order to support this analysis, quantitative phase contents were extracted from XRD data using Laine's theory [38]. By comparing the integrated intensities of different peaks in a specific spectrum, phase content can be achieved.

**Table 2** Calculated activation energies for gas-phase charged AZ91 and AZ31 for 14 h at 30 MPa and 300 °C

Examined Mg alloy	Heating rate (°C/min)	Peak's temperature ( $T_C$ ) (°C)	$E_a$ (kJ/mol)
AZ91	2	50	28 ± 8
	4	62	
	6	80	
	2	82	32 ± 15
	4	91	
	6	111	
	2	53	35 ± 3.5
	4	67	
	6	79	
AZ31	2	84	37 ± 13
	4	94	
	6	112	
	2	97	40 ± 14
	4	115	
	6	132	

$$V_{\text{MgH}_2} = \frac{I_\beta}{V_\alpha \cdot V_\beta} \quad (1.3)$$

where  $V_\beta$  is a certain phase content,  $I_\beta$  is a certain phase intensity, and  $R_\beta$  is a certain phase proportional factor. The denominator presents the multiplication of the rest of the phases in a sample by each other.

By assuming that all phase content is complete to one hundred, e.g.,  $V_{\alpha\text{-Mg}} + V_\beta + V_{\text{MgH}_2} = 100$ , the above equation can be rewritten as follows:

$$V_\beta = \frac{I_\beta}{\sum_{i=1}^n \frac{I_i}{R_i R_i}} \quad (1.4)$$

where  $n$  is the total number of phases in the sample.

Following the calculations of the phase contents, the content of  $\text{MgH}_2$  was about the same: up to ~2 wt% in both AZ91 and AZ31. This finding leads to the conclusion that the effects of the dehydrogenation process are highly dependent on  $\beta$ -phase.

In addition, the total amount of desorbed hydrogen from a certain heating rate was calculated according to the spectra's integration (integral of desorption rate on time), and the results are summarized in Table 3.

Differences between hydrogen's desorbed content at different heating rates are seen in both Mg alloys and are ascribed to the rapid desorption accompanied by faster kinetics when increasing heating rate. One major conclusion drawn from the results listed

**Table 3** Calculated hydrogen content for gas-phase charged AZ91 and AZ31 for 14 h at 30 MPa and 300 °C

Examined Mg alloy	Heating rate (°C/min)	Calculated desorbed hydrogen ±2 (%wt ppm)
AZ31	2	84
	4	62
	6	34
AZ91	2	25
	4	19
	6	8

in Table 3 is that AZ31 shows the highest desorbed hydrogen content compared with AZ91. A difference of ~70% was calculated for AZ31 at 2 °C/min heating rate, and this behavior repeats at different heating rates. Supported by previously published work on Mg lattice occupation [39], it can clearly be said that, because of the low hydrogen concentration (low peak intensity), hydrogen was mainly segregated into stress dislocations and field and grain boundaries. At high concentrations, hydrogen probably exceeds its solubility in Mg, and therefore,  $\text{MgH}_2$  hydride is formed. This indication is supported by  $\text{MgH}_2$ 's behavior in AZ31 and is demonstrated by the partial hydride decomposition in AZ91 compared with AZ31. At 2 °C/min of AZ31, almost all trapped hydrogen was able to be desorbed out (84%wt ppm H was desorbed out of the total content of 100%wt ppm H), and therefore, it can be concluded that the dehydrogenation process was almost complete. A comparison between remained trapped hydrogen at 2 °C/min, in AZ91 and AZ31, supports this indication: 75% compared with 16% trapped hydrogen contents were calculated for AZ91 and AZ31, respectively. A very important conclusion can be drawn based on these results, namely that  $\beta\text{-Mg}_{17}\text{Al}_{12}$  phase plays a fundamental role in the dehydrogenation reaction. Its high activation energy with hydrogen fastens  $\text{MgH}_2$  to it and increases the desorption temperature, and therefore, the reversible hydride process will be spontaneous only at temperatures higher than 300 °C.

## Summary and conclusions

The purpose of the current study was to investigate the role of alloying elements and microstructure on hydrogen trapping states and behavior of die-cast



AZ91 and rolled AZ31 Mg alloys. In both samples, the solute hydrogen was mainly segregated to stress dislocation fields at activation energies of  $\sim 28$  kJ/mol and  $\sim 35$  kJ/mole for AZ91 and AZ31, respectively, and grain boundaries at activation energies of  $\sim 32$  kJ/mol and  $\sim 37$  kJ/mole for AZ91 and AZ31, respectively. At a higher temperature level ( $\sim 300$  °C), additional trapping sites appeared, which was ascribed to the  $\beta$ -Mg<sub>17</sub>Al<sub>12</sub> phase. It was suggested that MgH<sub>2</sub> metal hydride was trapped adjacent to  $\beta$ -phase.

The fabrication process along with Al content had a major influence on microstructure, especially on the formation of the  $\beta$ -Mg<sub>17</sub>Al<sub>12</sub> phase, as well as on the dehydrogenating process. It was suggested that MgH<sub>2</sub> is formed adjacent to  $\beta$ -phase. It was proven that the reverse hydride reaction is highly dependent on the  $\beta$ -Mg<sub>17</sub>Al<sub>12</sub> phase. Due to the hydrogen embrittlement phenomenon, hydrogen cracking appeared only at AZ91, which contained the highest  $\beta$ -phase content. The embrittlement process was ascribed to the significant increment in AZ91-MgH<sub>2</sub> lattice volume ( $\sim 30\%$  increment). Differences were also seen in the content of desorbed hydrogen content, which was 70% higher in AZ31 compared with AZ91 and was ascribed to the lower amount of  $\beta$ -Mg<sub>17</sub>Al<sub>12</sub> in the former alloy. The negative effect of  $\beta$ -Mg<sub>17</sub>Al<sub>12</sub> was clearly shown to promote the hydrogen embrittlement process, in addition to preventing the dehydrogenating process. It can be concluded that high  $\beta$ -phase content (found in Mg alloys with  $<4\text{wt}\%$  Al content) in Mg alloys is less suitable for hydrogen storage material.

## Compliance with ethical standards

**Conflict of interest** The authors declare that they have no conflict of interest.

## References

- Eliezer D, Alves H (2002) Corrosion and oxidation of magnesium alloys. *Handb Mater Sel* 267–289
- For S, Distributors E (2000) Magnesium alloys development toward the 21st century. *Mater Sci Forum* 350–351:19–30. doi:10.4028/www.scientific.net/MSF.350
- Soenke S, Horst EF (2006) Automotive applications in Europe. *Magnes Technol* 499–569
- Kappes M, Iannuzzi M, Carranza RM (2013) Hydrogen embrittlement of magnesium and magnesium alloys: a review. *J Electrochem Soc* 160:168–178. doi:10.1149/2.023304jes
- Yuasa M, Nishihara D, Mabuchi M, Chino Yasumasa (2012) Hydrogen embrittlement in a magnesium grain boundary: a first-principles study. *J Phys Condens* 24:1–9. doi:10.1088/0953-8984/24/8/085701
- Song RG, Dietzel W, Zhang BJ et al (2004) Stress corrosion cracking and hydrogen embrittlement of an Al-Zn-Mg-Cu alloy. *Acta Mater* 52:4727–4743. doi:10.1016/j.actamat.2004.06.023
- Robertson IM, Sofronis P, Nagao A et al (2015) Hydrogen Embrittlement Understood. *Metall Mater Trans B* 46:1085–1103
- Minkovitz E, Talianker M, Eliezer D (1981) TEM investigation of hydrogen induced  $\epsilon$ -hcp-martensite in 316L-type stainless steel. *J Mater Sci* 16:3506–3508. doi:10.1007/BF00586316
- Scully, JR, Young, GA, Smith, SW (2012) Hydrogen embrittlement of aluminum and aluminum-based alloys. *Gaseous Hydrog embrittlement Mater Energy Technol* 707
- Silverstein R, Eliezer D (2016) Hydrogen trapping energy levels and hydrogen diffusion at high and low strain rates ( $\sim 10^5$  s<sup>-1</sup> and  $10^{-7}$  s<sup>-1</sup>) in lean duplex stainless steel. *Mater Sci Eng A* 674:419–427. doi:10.1016/j.msea.2016.08.019
- Silverstein R, Eliezer D, Glam B et al (2015) Evaluation of hydrogen trapping mechanisms during performance of different hydrogen fugacity in a lean duplex stainless steel. *J Alloys Compd* 648:601–608. doi:10.1016/j.jallcom.2015.07.029
- Sofronis P, Dadfarnia M, Novak P, et al (2009) A combined applied mechanics/materials science approach toward quantifying the role of hydrogen on material degradation. In: *Proc. 12th int. conf. fract. Ottawa, Canada*, pp 1–10
- Tal-Gutelmacher E, Eliezer D (2005) High fugacity hydrogen effects at room temperature in titanium based alloys. *J Alloys Compd* 404–406:613–616. doi:10.1016/j.jallcom.2004.12.172
- Choo WY, Lee JY (1982) Hydrogen trapping phenomena in carbon steel. *J Mater Sci* 17:1930–1938. doi:10.1007/BF00540409
- Abramov E, Eliezer D (1988) Trapping of hydrogen in helium-implanted metals. *J Mater Sci Lett* 7:108–110. doi:10.1007/BF01730586
- Shang CX, Bououdina M, Song Y, Guo ZX (2004) Mechanical alloying and electronic simulations of (MgH<sub>2</sub> + M) systems (M = Al, Ti, Fe, Ni, Cu and Nb) for hydrogen storage. *Int J Hydrogen Energy* 29:73–80. doi:10.1016/S0360-3199(03)00045-4
- Bouaricha S, Dodelet JP, Guay D et al (2000) Hydrogen behavior of Mg-Al and leached Mg-Al compounds prepared

- by high-energy ball-milling. *J Alloys Compd* 297:282–293. doi:[10.1016/S0925-8388\(99\)00612-X](https://doi.org/10.1016/S0925-8388(99)00612-X)
- [18] Renner J, Grabke HJ (1979) Determination of diffusion coefficients in the hydriding of alloys. *Chem Informationsd.* doi:[10.1002/chin.197903007](https://doi.org/10.1002/chin.197903007)
- [19] Ben-Haroush M, Ben-Hamu G, Eliezer D, Wagner L (2008) The relation between microstructure and corrosion behavior of AZ80 Mg alloy following different extrusion temperatures. *Corros Sci* 50:1766–1778. doi:[10.1016/j.corsci.2008.03.003](https://doi.org/10.1016/j.corsci.2008.03.003)
- [20] Ben-Hamu G, Eliezer D, Kaya A et al (2006) Microstructure and corrosion behavior of Mg-Zn-Ag alloys. *Mater Sci Eng A* 435–436:579–587. doi:[10.1016/j.msea.2006.07.109](https://doi.org/10.1016/j.msea.2006.07.109)
- [21] Nunes R, Adams JH, Ammons M, Al E (2001) Properties and selection: nonferrous alloys and special-purpose materials. *ASM Handb* 2:127–425
- [22] Silverstein R, Eliezer D, Glam B et al (2014) Influence of hydrogen on microstructure and dynamic strength of lean duplex stainless steel. *J Mater Sci* 49:4025–4031. doi:[10.1007/s10853-014-8075-9](https://doi.org/10.1007/s10853-014-8075-9)
- [23] Crank J (1975) *The mathematics of diffusion*, 2nd edn. Clarendon, Oxford
- [24] Atrens A, Winzer N, Song G et al (2006) Stress corrosion cracking and hydrogen diffusion in magnesium. *Adv Eng Mater* 8:749–751. doi:[10.1002/adem.200600050](https://doi.org/10.1002/adem.200600050)
- [25] Silverstein R, Eliezer D (2015) Hydrogen trapping mechanism of different duplex stainless steels alloys. *J Alloys Compd* 644:280–286. doi:[10.1016/j.jallcom.2015.04.176](https://doi.org/10.1016/j.jallcom.2015.04.176)
- [26] Silverstein R, Sobol O, Boellinghaus T et al (2016) Hydrogen behavior in SAF 2205 duplex stainless steel. *J Alloys Compd* 659:2689–2695. doi:[10.1016/j.jallcom.2016.11.184](https://doi.org/10.1016/j.jallcom.2016.11.184)
- [27] Lee S, Lee J (1986) The trapping and transport phenomena of hydrogen in nickel. *Metall Trans A* 17:181–187
- [28] Turnbull A, Hutchings RB, Ferriss DH (1997) Modelling of thermal desorption of hydrogen from metals. *Mater Sci Eng* 238:317–328
- [29] Stampfer JF, Holley CE, Suttle JF (1960) The magnesium-hydrogen system. *J Am Chem Soc* 82:3504–3508. doi:[10.1021/ja01499a006](https://doi.org/10.1021/ja01499a006)
- [30] Chen J, Ai M, Wang J et al (2009) Formation of hydrogen blister on AZ91 magnesium alloy during cathodic charging. *Corros Sci* 51:1197–1200. doi:[10.1016/j.corsci.2009.02.020](https://doi.org/10.1016/j.corsci.2009.02.020)
- [31] Chen J, Wang J, Han E et al (2008) States and transport of hydrogen in the corrosion process of an AZ91 magnesium alloy in aqueous solution. *Corros Sci* 50:1292–1305. doi:[10.1016/j.corsci.2008.01.028](https://doi.org/10.1016/j.corsci.2008.01.028)
- [32] Schober T (1981) The magnesium-hydrogen system: transmission electron-microscopy. *Metall Trans A* 12A:951–957. doi:[10.1007/bf02643475](https://doi.org/10.1007/bf02643475)
- [33] Ghali E (2011) Magnesium and magnesium alloys. In: Winston R (ed) *Uhlig's corrosion handbook*, 3rd edn. Wiley, New York, pp 809–836
- [34] Smith WF, Hashemi J (2009) *Foundation of materials science and engineering*, Chap 8, 4th edn. pp 318–321
- [35] Turnbull A, Hutchings RB (1994) Analysis of hydrogen atom transport in a two-phase alloy. *Mater Sci Eng A* 177:161–171. doi:[10.1016/0921-5093\(94\)90488-X](https://doi.org/10.1016/0921-5093(94)90488-X)
- [36] Eliezer D, Tal-Gutelmacher E, Cross CE, Boellinghaus T (2006) Hydrogen trapping in  $\beta$ -21S titanium alloy. *Mater Sci Eng A* 421:200–207. doi:[10.1016/j.msea.2006.01.067](https://doi.org/10.1016/j.msea.2006.01.067)
- [37] Tal-Gutelmacher E, Eliezer D, Abramov E (2007) Thermal desorption spectroscopy (TDS)—Application in quantitative study of hydrogen evolution and trapping in crystalline and non-crystalline materials. *Mater Sci Eng A* 445–446: 625–631. doi:[10.1016/j.msea.2006.09.089](https://doi.org/10.1016/j.msea.2006.09.089)
- [38] Laine ESU (1978) A high-speed determination of the volume fraction of ferrite in austenitic stainless steel by EDXRD. *J Phys F Met Phys* 8:1343–1348. doi:[10.1088/0305-4608/8/7/007](https://doi.org/10.1088/0305-4608/8/7/007)
- [39] Chino Y, Nishihara D, Ueda T, Mabuchi M (2011) Effects of hydrogen on the mechanical properties of pure magnesium. *Mater Trans* 52:1123–1126. doi:[10.2320/matertrans.MC201009](https://doi.org/10.2320/matertrans.MC201009)